ADVANCED ENERGY MATERIALS
www.advenergymat.de

Revealing the Short-Circuiting Mechanism of Garnet-Based Solid-State Electrolyte

*Yongli Song, Luyi Yang, Wenguang Zhao, Zijian Wang, Yan Zhao, Ziqi Wang, Qinghe Zhao, Hao Liu, and Feng Pan**

Garnet-type solid-state electrolytes (SSEs) have been widely studied as a promising candidate for Li metal batteries. Despite the common belief that inorganic SSEs can prevent dendrite propagation, garnet SSEs suffer from relatively low critical current density (CCD) at which the SSEs are abruptly short-circuited by Li dendrites. In this study, the short-circuiting mechanism of garnet $Li_7La_{2.75}Ca_{0.25}Zr_{1.75}Nb_{0.25}O_{12}$ (LLCZN) is investigated. It is found that instead of propagating uniaxially from one electrode to other in a dendritic form, metallic lithium is formed within the SSE. This can be attributed to the fact that electrons combine with Li ions at the grain boundary, which exhibits relatively high electronic conductivity, and then reduce Li^+ to Li^0 to cause short circuits. In order to reduce the electronic conductivity at the grain boundary, a thin layer of $LiAlO_2$ is coated on the grain surface of LLCZN, which results in an improved CCD value. It is also found that under higher external voltages, the electronic conductivity of SSE becomes more significant, which is believed to be the origin of CCD. These findings not only shed light on the short-circuiting mechanism of garnet-type SSEs but also offer a novel perspective and useful guidance on their designs and modifications.

1. Introduction

Li metal anodes, featuring both high volumetric and gravimetric energy densities, have attracted great attention due to the demand for high-energy batteries in portable electrical devices and electric vehicles in the past decade.[1,2] However, the detrimental Li dendrites may cause short circuits in a battery, triggering battery fire/explosion. Consequently, the application of Li metal in a conventional lithium ion battery is limited.[3] Solid-state electrolytes (SSEs) have attracted wide attention due to their excellent safety properties and better cycling stability. A range of SSEs, such as perovskite-type,[4] antiperovskite-type,[5] thio-LiSICON-type,[6] NASICON-type,[7] garnet,[8] and sulfide-based glass/ceramic,[9] have been investigated in the past decade. Among these SSEs, garnet with nominal composition $Li_7La_3Zr_2O_{12}$ (LLZO) is one of the most promising solid electrolytes.[10] LLZO exhibits high ionic conductivity (10^{-4}–10^{-3} S cm^{-1}),[11] good electrochemical stability,[12] and high chemical stability compared to Li metal.[13] Moreover, it exhibits relatively high elastic (≈150 GPa) and shear (≈60 GPa) moduli, which are considered crucial in suppressing the propagation of Li dendrites.[14] However, previous results have shown that garnet SSEs generally suffer from low critical current density (CCD)[15–18] due to which short circuits occur abruptly.[19] This phenomenon largely contradicts their expectations, and hence, the origin of low CCD values still remains unclear. In addition, it is widely believed that the mechanism of short-circuiting in garnet SSEs is similar to that in liquid electrolytes, where Li dendrites first nucleate at the Li/electrolyte interface,[3] and then propagate along the grain boundaries or through the voids between ceramic particles.[20] By far, the current studies have focused mainly on the modification of the Li/SSE interface by facilitating a better contact.[21–23] However, the existence of CCD cannot be explained through the gradually propagating model.

In this work, the short-circuiting mechanism of garnet $Li_7La_{2.75}Ca_{0.25}Zr_{1.75}Nb_{0.25}O_{12}$ (LLCZN) has been studied. We have found that low CCD is attributed to high electronic conductivity at the grain boundaries, where electrons reduce Li ions, thereby forming metallic Li. Consequently, a new short-circuiting model is proposed in which metallic lithium is formed simultaneously within an SSE instead of growing uniaxially. Furthermore, a thin layer of $LiAlO_2$ (LAO) is coated on the grain surface of LLCZN, which results in an improved CCD value.

2. Results and Discussion

The X-ray diffraction (XRD) pattern (Figure S1a, Supporting Information) of as-prepared LLCZN can be well indexed to the reference pattern of standard $Li_5La_3Nb_2O_{12}$ with the cubic garnet phase (PDF 80-0457), suggesting high purity of the product. The lattice fringes corresponding to the (310) plane of LLCZN can be observed from the transmission electron

Dr. Y. Song, Dr. L. Yang, W. Zhao, Z. Wang, Y. Zhao, Dr. Z. Wang, Dr. Q. Zhao, H. Liu, Prof. F. Pan
School of Advanced Materials
Peking University
Shenzhen Graduate School
Shenzhen 518055, P. R. China
E-mail: panfeng@pkusz.edu.cn
The ORCID identification number(s) for the author(s) of this article can be found under https://doi.org/10.1002/aenm.201900671.

DOI: 10.1002/aenm.201900671

microscopy (TEM) image shown in Figure S1b (Supporting Information), which indicates that a highly crystalline LLZO mother powder is obtained. Figure S1c (Supporting Information) shows that after sintering, the cross section of the LLCZN pellet demonstrate a dense microstructure with density of 4.83 g cm^{-3} measured using the Archimedes method. The ionic conductivity of the LLCZN electrolyte is calculated using the impedance spectroscopy shown in Figure S1d (Supporting Information). As a result, the ionic conductivity of LLCZN is measured to be 1.25×10^{-4} S cm^{-1} at 25 °C. Note that the preparation method of solid electrolytes and the testing conditions may vary widely with different studies, which can lead to different solid electrolytes. For instance, the hot-pressing method can be used to achieve denser SSE pellets, however, it is beyond the scope of this work.

The Li plating/stripping performances of LLCZN were investigated during galvanostatic cycling at room temperature in a Li/LLCZN/Li symmetric cell. In this work, a minimum amount (3 µL) of the liquid electrolyte (1 M LiFSI in DME) is added between Li and SSE to achieve fully wetted interfaces without permeating them into the ceramics. **Figure 1**a shows that stable Li plating/stripping behavior can be observed for 200 h during cycling at the current density of 0.1 mA cm^{-2}; whereas when a higher current density is applied, the cell was short-circuited after merely 0.2 h (Figure 1b), which is confirmed by the electrochemical impedance spectroscopy (EIS) data presented in Figure S2 (Supporting Information). To explore the origin of short-circuiting in SSEs, the SSE pellets are carefully examined after galvanostatic cycling. As shown in Figure 1c, small metallic lithium domains (dark spots) are clearly observed at the cross section of the pellets cycled at low current density (0.1 mA cm^{-2}). In contrast, the metallic Li domains in the cross section of the pellets cycled at 0.4 mA cm^{-2} (Figure 1d) are much larger. The scanning electron microscopy (SEM) image of cycled LLCZN in the back-scattered electron (BSE) mode (Figure S3, Supporting Information) also confirms this observation. It can be inferred from the difference between Figure 1c,d that short-circuiting is caused by metallic lithium present within the SSE. However, instead of the widely perceived "penetration" model in which Li dendrite grows from one end to the other, spots that represent metallic Li are independently and randomly dispersed in LLCZN, suggesting that the formation of metallic Li can also occur within the SSE. As a result, a new mechanism is proposed here in which Li ions are reduced by electrons that travel from Li metal during lithium plating, forming Li^0 within LLCZN.

To validate this hypothesis, a different cell configuration is adopted using the Si–C composite cathode. **Figure 2**a shows

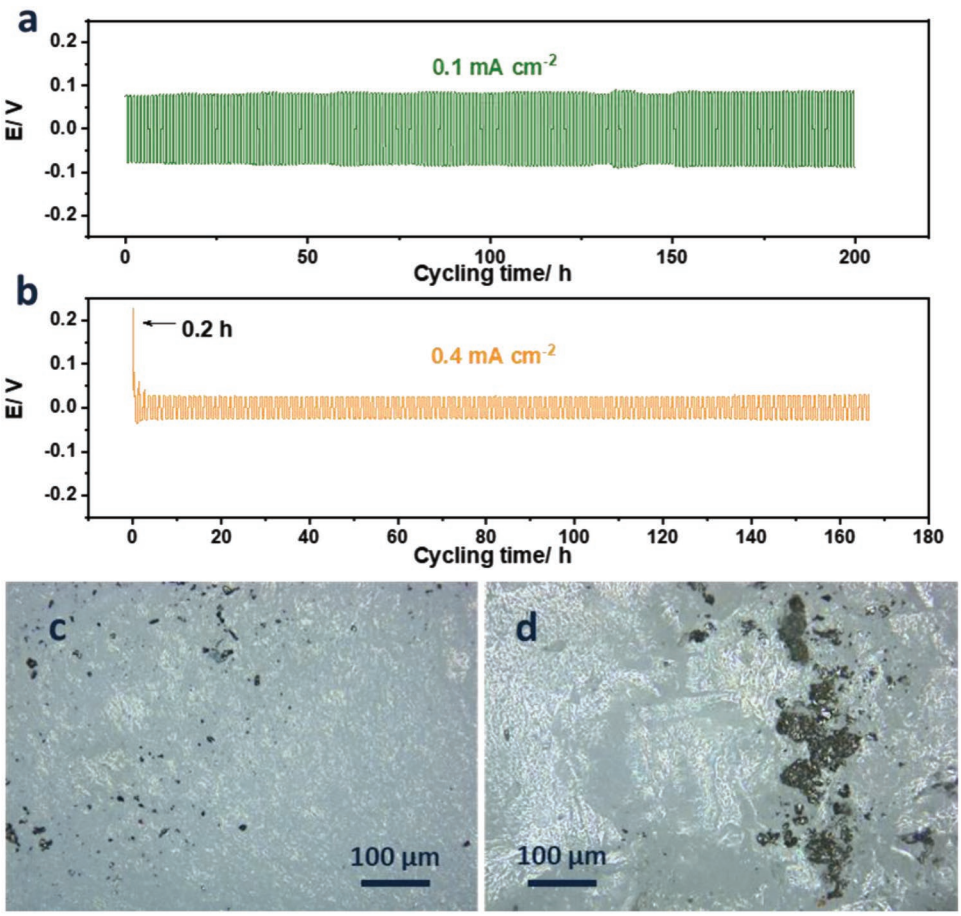

Figure 1. Potential profiles of Li/LLCZN/Li cell during galvanostatic cycling at the current densities of a) 0.1 mA cm^{-2} and b) 0.4 mA cm^{-2}. Optical images of the cross section of cycled LLCZN at the current densities of c) 0.1 mA cm^{-2} and d) 0.4 mA cm^{-2}.

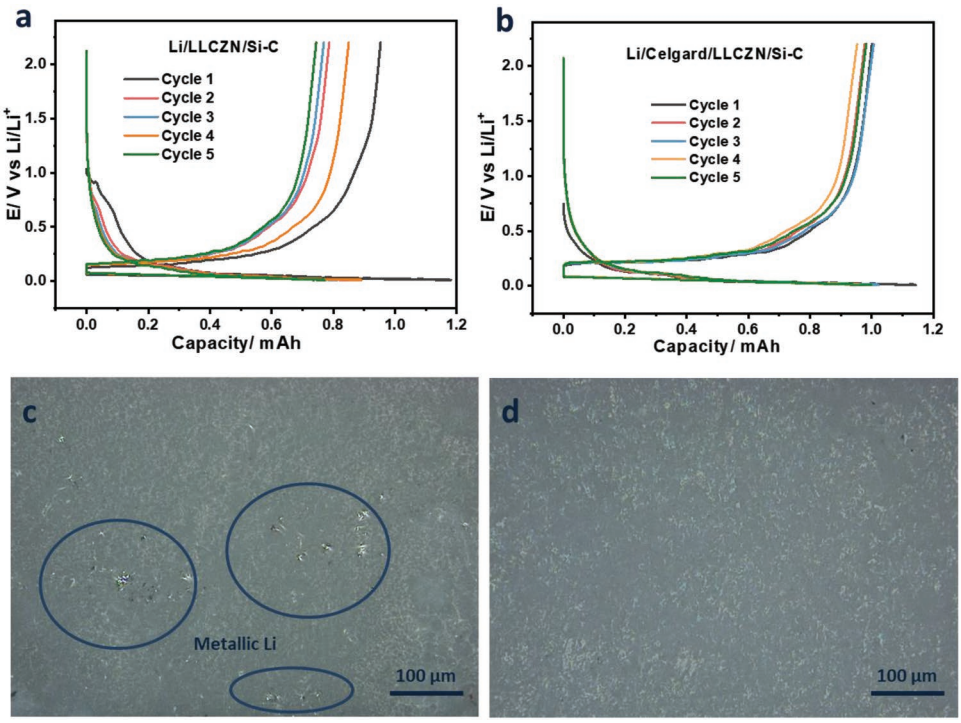

Figure 2. Voltage profiles of a) Li/LLCZN/Si–C and b) Li/Celgard/LLCZN/Si-C cells for different cycle numbers at the current density of 0.1 mA cm^{-2}. Optical images of the cross sections of cycled LLCZN a) without and b) with a Celgard 2400 separator.

that low coulombic efficiency can be observed at each cycle (detailed data are presented in Figure S4, Supporting Information) by continuously charging and discharging the Li/LLCZN/Si–C cell, indicating lithium loss during the charging (lithium plating) process. In order to cut off the electron pathway, a Celgard 2400 separator is placed between Li and LLCZN. Note that a minimum amount of the electrolyte (10 μL) is added in both experiments to ensure that the interfaces are equally wetted in the same way as the cell without a separator (Figure S5, Supporting Information), and hence, the ion transfer will not be a limiting factor. As shown in Figure 2b, the charging capacities are well retained after five cycles. To determine the origin of the differences in the results shown in Figure 2a,b, the cross sections of both SSEs are examined after cycling. It can be seen clearly from Figure 2c, d that when LLCZN is contacted directly with lithium anode, Li^0 is formed within the solid electrolyte; whereas, after the electron pathway is greatly hindered by a piece of an electronic insulating separator, no obvious Li^0 domain is observed. Therefore, the lithium loss, shown in Figure 2a, can be attributed to the formation of Li^0 in the SSE, and this process is highly dependent on the electron transfer from the Li metal anode.

According to previous research,[24,25] the electronic conductivity in several ceramics is mainly contributed by the grain boundaries of SSEs. It is also predicted by performing computational simulations that the grain boundaries of garnet-type SSE can provide additional electronic pathways for electrons.[26] In addition, metallic Li is generally reported to be found either at the grain boundaries or the voids of SSEs.[27,28] In this study, it can be reasonably assumed that Li^0 is most likely to form at the grain boundaries as no visible voids are found in the LLCZN pellet (Figure S1c, Supporting Information). In order to experimentally verify this assumption, a thin layer of $LiAlO_2$ (LAO) is coated on LLCZN powder using the facile chemical coating process (details are described in the experimental section) to achieve a low electronic conductivity at the grain boundary. To confirm whether LAO is successfully coated on LLCZN particles, the product (LLCZN@LAO) is examined using TEM. Figure S6 (Supporting Information) shows that a coating layer is formed at the particle surface of LLCZN, and **Figure 3**a further demonstrates lattice fringes corresponding to (211) and (201) planes of LAO (PDF 73-1338, space group P41212). In addition, as shown in Figure 3b, after etching the surface of LLCZN@LAO pellets with a focused ion beam (FIB), the exposed area exhibits a very low content of Al compared to La element. This further proves that LAO is coated on the surface of LLCZN instead of doped into LLCZN. In addition, X-ray photoelectron spectra, shown in Figure S7 (Supporting Information), also demonstrates that the surface of LLCZN@LAO is covered with an Al-rich layer, which can be etched away by an Ar ion, revealing the bulk of LLCZN. This result indicates the successful coating of LAO on the surface of LLCZN particles. Figure 3c demonstrates that the XRD patterns of both LLCZN and LLCZN@LAO are exactly the same, suggesting no phase changes during the coating process. Moreover, no impurity peaks are found in LLCZN@LAO ceramics due to very small content of LAO (≈1.3 wt%). The ionic conductivity of LLCZN@LAO is measured to be 1.23×10^{-4} S cm^{-1} at 25 °C (Figure S8, Supporting Information), which is very close to LLCZN, indicating that despite the low ionic conductivity of LAO, the coating layer does not impede the transfer of Li ions between grain boundaries.

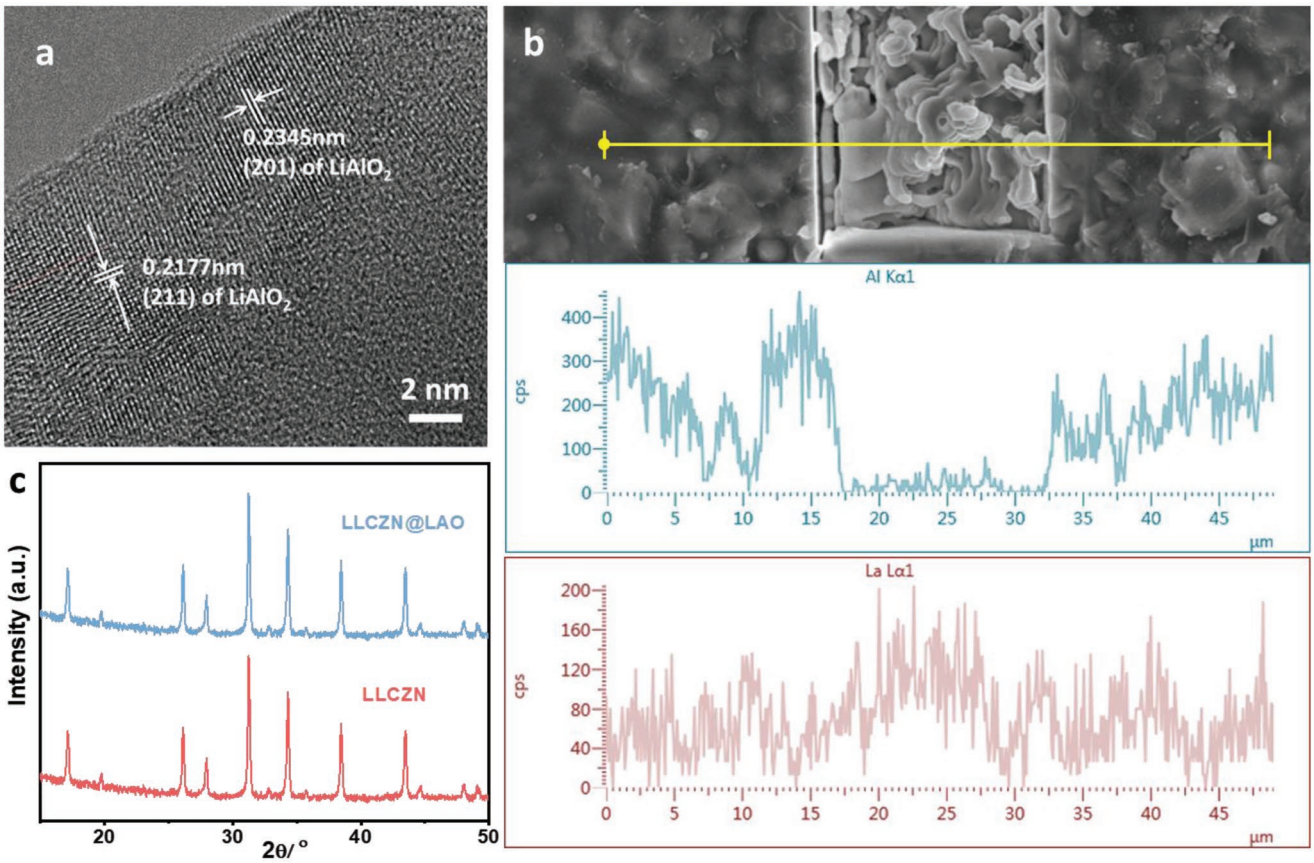

Figure 3. a) TEM image of LLCZN@LAO. b) SEM-EDS analysis of LLCZN@LAO pellet, whose surface is etched by FIB. c) XRD patterns of LLCZN and LLCZN@LAO.

Figure S9a (Supporting Information) shows that LLCZN@LAO exhibits much lower area specific resistance (ASR) (25 Ω cm^2) with Li metal compared to LLCZN (4100 Ω cm^2). This result is similar to a previous work in which a thin while controllable Al_2O_3 layer was directly coated on the external surface of a solid electrolyte using the atomic layer deposition (ALD) technique. Such a coating layer exhibits a highly lithiophilic feature and a low ASR (1 Ω cm^2), resulting in homogeneous Li plating/stripping, and hence, an improved CCD.[22] Therefore, the reduced ASR of LLCZN@LAO indicates that a modification layer of LAO is not only formed at the grain boundaries, but also at the interface between Li and SSE pellet, which facilitates a well-wetted Li-SSE interface. Because ASR is a critical factor in the evaluation of CCD, the effects of ASR should be excluded by creating equally wetted interfaces for both LLCZN and LLCZN@LAO in order to independently study the effect of the modification layer of LAO on grain boundaries. Previous studies have shown that applying a liquid electrolyte[29] and a gel electrolyte[30] can efficiently reduce interface resistance between Li and SSEs. As shown in Figure S9b (Supporting Information), the interfacial ASR of LLCZN and LLCZN@LAO with Li metal are reduced from 4100 Ω cm^2 and 25 Ω cm^2 to 16 Ω cm^2 and 14 Ω cm^2, respectively. Consequently, the grain boundaries can be investigated separately. After galvanostatic cycling with step-up current densities, the CCD values of LLCZN and LLCZN@LAO are measured to be 0.4 and 0.75 mA cm^{-2}, respectively, as shown in **Figure 4**a,b. In addition, the electronic conductivity of SSEs is measured using the chronoamperometry method in which a constant voltage is applied versus the open circuit potential (OCP), and a steady-state current (I_s) is obtained. Next, the electronic conductivity is calculated according to Ohm's Law. As shown in the inset of Figure 4c, the electronic conductivity of LLCZN (3.59×10^{-8} S cm^{-1}) is measured to be higher than that of LLCZN@LAO (1.01×10^{-8} S cm^{-1}), indicating different CCD values that originated due to their different electronic conductivities. By examining the electronic conductivity at various applied voltages (Figure 4c), it is observed that at lower voltages, the value of I_s first increases linearly, indicating a constant electronic conductivity. However, as higher voltages are applied, I_s eventually becomes nonlinear, indicating increasing electronic conductivity. This phenomenon can also qualitatively explain the reason for low CCD of garnet SSEs: a higher current flowing through the SSE generally leads to a higher polarization voltage; therefore, at some point, as the polarization voltage is sufficiently high, the grain boundaries of the SSE can become electronic conductive and allow relatively "free" electron transfer within the SSE. In other words, the short-circuiting phenomenon is more dependent on the "critical applied voltage" than "critical current density." This also explains the significance of determining ASR at the Li/SSE interface as with a low ASR,[22] a lower external voltage can be achieved at the same current density. Furthermore, it is

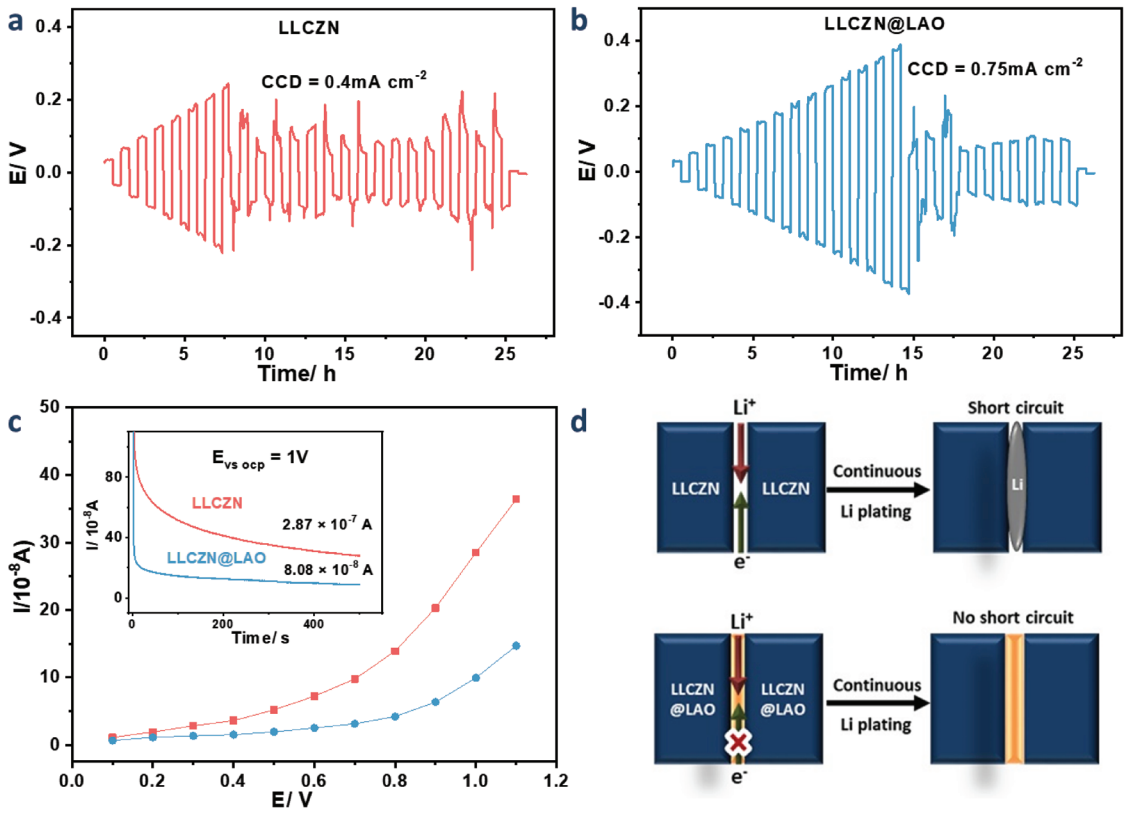

Figure 4. Lithium platting/stripping performance of a) LLCZN and b) LLCZN@LAO in Li symmetric cells at different current densities. c) Values of I_s for LLCZN and LLCZN@LAO with different applied external voltages; Chronoamperometry results of LLCZN and LLCZN@LAO with an applied external voltage of 1 V (inset). d) Schematic illustrations of Li formation within LLCZN and how to suppress it through surface coating.

also observed that after coating a thin insulating buffer layer (i.e., LAO) at the grain boundary, the nonlinear tendency of I_s can be suppressed effectively, thereby achieving a higher CCD value (Figure 4d). It is also noteworthy that when current densities of 0.35 mA cm^{-2} and 0.375 mA cm^{-2} are applied, as shown in Figure S10 (Supporting Information), short-circuiting still occurs as long as the cells are cycled long enough. This indicates that although CCD represents a specific value, the formation of Li° can occur at slightly lower current densities. In this scenario, the short-circuiting process depends on the kinetics of the nucleation and growth of metallic Li domain within the SSE.

3. Conclusion

In this work, we have studied the short-circuiting mechanism of garnet SSE (LLCZN). Instead of growing uniaxially from one electrode as lithium dendrite, metallic lithium is formed at the grain boundary of LLCZN. This is because electrons can travel along the grain boundary of LLCZN, which exhibits high electronic conductivity, and reduce Li^+ into Li^0. In order to reduce the electronic conductivity at the grain boundary, a thin layer of $LiAlO_2$ (LAO) is coated on the grain surface of LLCZN, which results in an improved CCD value. It is also found that when external voltage is sufficiently high, the electronic conductivity of the SSE becomes more significant, which explains the origin of CCD. These results show that apart from directly coating a modification layer on SSE pellets, which can effectively reduce ASR and suppress inhomogeneous Li plating/stripping,[22] supplementary approaches such as reducing electronic conductivity by grain boundary coating are equally effective in order to further improve the CCD of garnet SSEs.

4. Experimental Section

$Li_7La_{2.75}Ca_{0.25}Zr_{1.75}Nb_{0.25}O_{12}$ (LLCZN) Powder Preparation: Garnet-structured LLCZN was synthesized in which the simultaneous substitution of the La^{3+} site with Ca^{2+} and the Zr^{4+} site with Nb^{5+} reduced sintering temperature, steady cubic garnet phase, and increased conductivity of the Li ion.[19] Suitable amounts of Li_2CO_3 (99.99% Alfa with 10% excess to compensate the sintering loss), La_2O_3 (99.99% Al), $CaCO_3$ (99.99% Alfa), ZrO_2 (99.99% Alfa), and Nb_2O_5 (99.99% Al) precursors were mixed using the ball milling process with a ZrO_2 jar and balls for 10 h. The mixture was calcined at 900 °C for 10 h to obtain mother LLCZN powder.

$LiAlO_2$ (LAO) Modification on Electrodes: In order to prepare LLCZN@LAO, the as-prepared LLCZN mother powder, 4 wt% aluminum isopropanol, and 1.5 wt% lithium acetate (with 20% excess to compensate the sintering loss) were put into isopropanol. After mixing to dry, the mixed powder was calcined at 500 °C for 6 h to achieve LLCZN powder with the coating of the amorphous layer of LAO (LLCZN@LAO). The LLCZN and LLCZN@LAO powders were pressed into pellets of diameter 1/2 in., and the white pellets buried with mother powders were

sintered in alumina crucible at 1100 °C for 10 h. The resulting pellets were polished using a sand paper to achieve thickness of ≈1 mm, and then stored in Ar-filled glove box to prevent reaction with humidity and CO_2.

Si–C Electrode Preparation: The Si–C anode material (S420, Beiterui) was mixed with styrene-butadiene rubber (SBR), carboxymethyl cellulose (CMC), and acetylene black in a weight ratio of 92:2:2:3. The mixture was then stirred and dispersed in water to form the cathode slurry. The obtained slurry was then casted on a copper foil, dried at room temperature, and was then cut into pellets of diameter 12 mm. The pellets were further dried overnight at 120 °C in a vacuum.

Characterization and Electrochemical Measurement: The structural characterization was performed using XRD (Bruker D8 Advance powder X-ray diffractometer) with 2θ in the range of 10°–50° with a step size of 0.02°. The FIB sectioning of craters was carried out on an FIB microscope (FEI Scios) using the incident beam energy of 30 kV Ga+. Morphology study and element distribution were conducted by SEM (Zeiss SUPRA-55), TEM (JEM-3200FS, JEOL), and 3D laser scanning confocal microscopy (LSCM, VK-X200, KEYENCE). X-ray photoelectron spectroscopy (XPS, ESCALab220I-XL) was conducted to measure the chemical properties. The ionic conductivity was calculated from data collected using an electrochemical workstation (CHI 660E) in the frequency range from 1 MHz to 1 Hz with amplitude of 5 mV at room temperature. A symmetric cell was assembled by stacking LLCZN/LLCZN@LAO between two Li foils in a Swagelok cell. The lithium plating/stripping test was carried out during galvanostatic cycling using an automatic galvanostatic charge–discharge unit (Maccor, MC-16 Battery Test System) at room temperature. The DC polarization measurements to achieve electronic conductivity of the solid electrolyte were performed using an electrochemical workstation (1400 cell test system, Solartron) with an applied voltage of 0.7 V (open-circuit voltage *V*s) at room temperature.

Supporting Information

Supporting Information is available from the Wiley Online Library or from the author.

Acknowledgements

Y.S. and L.Y. contributed equally to this work. This work was financially supported by grants from the National Key R&D Program of China (2016YFB0700600), Guangdong Innovation Team Project (No. 2013N080), Shenzhen Science and Technology Research Grant (JCYJ20160531141048950), and Guangdong Key Lab Project (No. 2017B0303010130).

Conflict of Interest

The authors declare no conflict of interest.

Keywords

critical current density, garnet electrolytes, grain boundaries, interfacial modifications, solid-state batteries

Received: February 26, 2019
Published online: April 8, 2019

[1] D. Lin, Y. Liu, Y. Cui, *Nat. Nanotechnol.* **2017**, *12*, 194.
[2] J. Lu, Z. Chen, F. Pan, Y. Cui, K. Amine, *Electrochem. Energy Rev.* **2018**, *1*, 35.
[3] W. Xu, J. Wang, F. Ding, X. Chen, E. Nasybulin, Y. Zhang, J. G. Zhang, *Energy Environ. Sci.* **2014**, *7*, 513.
[4] J. F. Ihlefeld, P. G. Clem, B. L. Doyle, P. G. Kotula, K. R. Fenton, C. A. Apblett, *Adv. Mater.* **2011**, *23*, 5663.
[5] X. Lü, J. W. Howard, A. Chen, J. Zhu, S. Li, G. Wu, P. Dowden, H. Xu, Y. Zhao, Q. Jia, *Adv. Sci.* **2016**, *3*, 1500359.
[6] S. Muy, J. C. Bachman, L. Giordano, H. H. Chang, D. L. Abernathy, D. Bansal, O. Delaire, S. Hori, R. Kanno, F. Maglia, S. Lupart, P. Lamp, Y. Shao-Horn, *Energy Environ. Sci.* **2018**, *11*, 850.
[7] Y. Noda, K. Nakano, H. Takeda, M. Kotobuki, L. Lu, M. Nakayama, *Chem. Mater.* **2017**, *29*, 8983.
[8] L. Buannic, B. Orayech, J.-M. López Del Amo, J. Carrasco, N. A. Katcho, F. Aguesse, W. Manalastas, W. Zhang, J. Kilner, A. Llordés, *Chem. Mater.* **2017**, *29*, 1769.
[9] Y. Kato, S. Hori, T. Saito, K. Suzuki, M. Hirayama, A. Mitsui, M. Yonemura, H. Iba, R. Kanno, *Nat. Energy* **2016**, *1*, 16030.
[10] H. Duan, H. Zheng, Y. Zhou, B. Xu, H. Liu, *Solid State Ionics* **2018**, *318*, 45.
[11] R. Murugan, V. Thangadurai, W. Weppner, *Angew. Chem., Int. Ed.* **2007**, *46*, 7778.
[12] T. Thompson, S. Yu, L. Williams, R. D. Schmidt, R. Garcia-Mendez, J. Wolfenstine, J. L. Allen, E. Kioupakis, D. J. Siegel, J. Sakamoto, *ACS Energy Lett.* **2017**, *2*, 462.
[13] V. Thangadurai, D. Pinzaru, S. Narayanan, A. K. Baral, *J. Phys. Chem. Lett.* **2015**, *6*, 292.
[14] J. E. Ni, E. D. Case, J. S. Sakamoto, E. Rangasamy, J. B. Wolfenstine, *J. Mater. Sci.* **2012**, *47*, 7978.
[15] X. B. Cheng, T. Z. Hou, R. Zhang, H. J. Peng, C. Z. Zhao, J. Q. Huang, Q. Zhang, *Adv. Mater.* **2016**, *28*, 2888.
[16] C. Ma, Y. Cheng, K. Yin, J. Luo, A. Sharafi, J. Sakamoto, J. Li, K. L. More, N. J. Dudney, M. Chi, *Nano Lett.* **2016**, *16*, 7030.
[17] R. Raj, J. Wolfenstine, *J. Power Sources* **2017**, *343*, 119.
[18] A. Sharafi, H. M. Meyer, J. Nanda, J. Wolfenstine, J. Sakamoto, *J. Power Sources* **2016**, *302*, 135.
[19] A. Sharafi, C. G. Haslam, R. D. Kerns, J. Wolfenstine, J. Sakamoto, *J. Mater. Chem. A* **2017**, *5*, 21491.
[20] F. Aguesse, W. Manalastas, L. Buannic, J. M. L. Del Amo, G. Singh, A. Llordés, J. Kilner, *ACS Appl. Mater. Interfaces* **2017**, *9*, 3808.
[21] L. Yang, Z. Wang, Y. Feng, R. Tan, Y. Zuo, R. Gao, Y. Zhao, L. Han, Z. Wang, F. Pan, *Adv. Energy Mater.* **2017**, *7*, 1.
[22] X. Han, Y. Gong, K. Fu, X. He, G. T. Hitz, J. Dai, A. Pearse, B. Liu, H. Wang, G. Rubloff, Y. Mo, V. Thangadurai, E. D. Wachsman, L. Hu, *Nat. Mater.* **2017**, *16*, 572.
[23] Y. Li, B. Xu, H. Xu, H. Duan, X. Lü, S. Xin, W. Zhou, L. Xue, G. Fu, A. Manthiram, J. B. Goodenough, *Angew. Chem., Int. Ed.* **2017**, *56*, 753.
[24] X. Guo, J. Fleig, J. Maier, *J. Electrochem. Soc.* **2001**, *148*, J50.
[25] M. J. Verkerk, B. J. Middelhuis, A. J. Burggraaf, *Solid State Ionics* **1982**, *6*, 159.
[26] H. K. Tian, B. Xu, Y. Qi, *J. Power Sources* **2018**, *392*, 79.
[27] M. Nagao, A. Hayashi, M. Tatsumisago, T. Kanetsuku, T. Tsuda, S. Kuwabata, *Phys. Chem. Chem. Phys.* **2013**, *15*, 18600.
[28] E. J. Cheng, A. Sharafi, J. Sakamoto, *Electrochim. Acta* **2017**, *223*, 85.
[29] X. Chen, T. Wang, W. Lu, T. Cao, M. Xue, B. Li, C. Zhang, *J. Alloys Compd.* **2018**, *744*, 386.
[30] B. Liu, Y. Gong, K. Fu, X. Han, Y. Yao, G. Pastel, C. Yang, H. Xie, E. D. Wachsman, L. Hu, *ACS Appl. Mater. Interfaces* **2017**, *9*, 18809.